water

Supplementary Materials

Assessment of the Future Impact of Climate Change on the Hydrology of the Mangoky River, Madagascar Using ANN and SWAT

Table S1. List of predictors from NCEP/NCAR.

n°	Code	Description	n°	Code	Description
1	mslp	Mean sea level pressure	14	p8_f	Geostrophic airflow velocity at 850 hPa
2	p_f	Geostrophic airflow velocity near the surface	15	p8_u	Zonal velocity component at 850 hPa
3	p_u	Zonal velocity component near the surface	16	p8_v	Meridional velocity component at 850 hPa
4	p_v	Meridional velocity component near the surface	17	p8_z	Vorticity at 850 hPa
5	p_z	Vorticity near the surface	18	p8th	Wind direction at 850 hPa
6	p_th	Wind direction near the surface	19	p8zh	Divergence at 850 hPa
7	p_zh	Divergence near the surface	20	p500	500 hPa geopotential height
8	p5_f	Geostrophic airflow velocity at 500 hPa	21	p850	850 hPa geopotential height
9	p5_u	Zonal velocity component at 500 hPa	22	r500	Relative humidity at 500 hPa height
10	p5_v	Meridional velocity component at 500 hPa	23	R850	Relative humidity at 850 hPa height
11	p5_z	Vorticity at 500 hPa	24	rhum	Near surface relative humidity
12	p5th	Wind direction at 500 hPa	25	shum	Near surface specific humidity
13	p5zh	Divergence at 500 hPa	26	temp	Near surface air temperature

Figure S1 shows the land use and land cover in the Mangoky watershed. According to Figure S1, the land in the Mangoky includes Pasture (PAST), row crop (AGRR), grasslands/herbaceous (RNGE), range shrubland (RNGB), deciduous forest (FRSD), evergreen forest (FRSE), water (WATR), and barren (BARR). The land use classification is mainly range shrubland with 28395km^2, accounting for 75.95% of the total area, followed by grasslands/herbaceous with 5218km^2 accounting for 13.96% of the total land area. Pasture occupies 4.50% of the total area with 1681km^2, and the deciduous forest occupies 2.83% of the total area with 1057km^2. The rest of the land is water, row crop, and barren with 1.1%, 0.89%, and 0.35% accounting for 410km^2, 233km^2, and 129km^2, respectively.

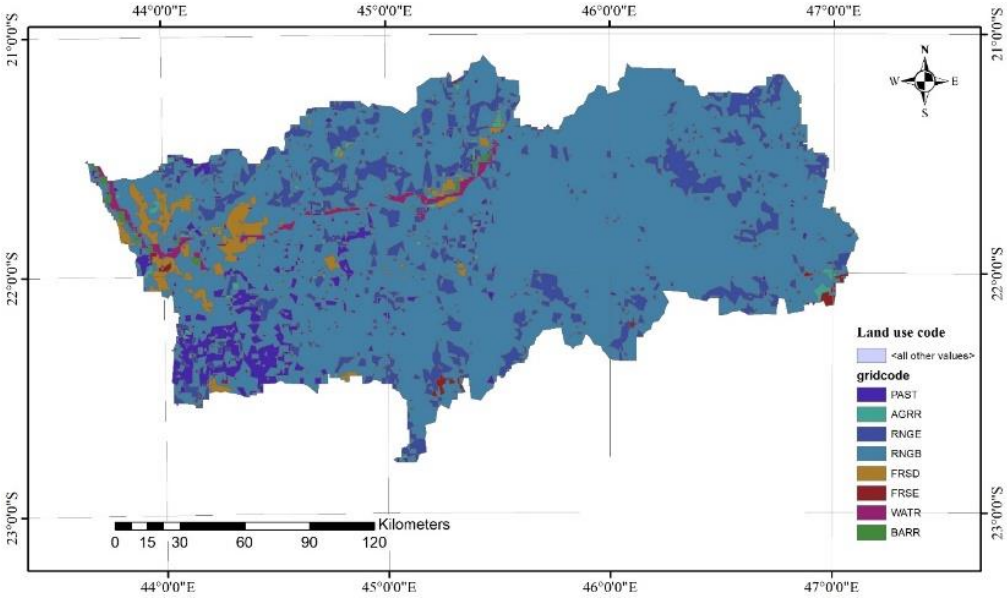

Figure S1. Land use and land cover in the Mangoky basin.

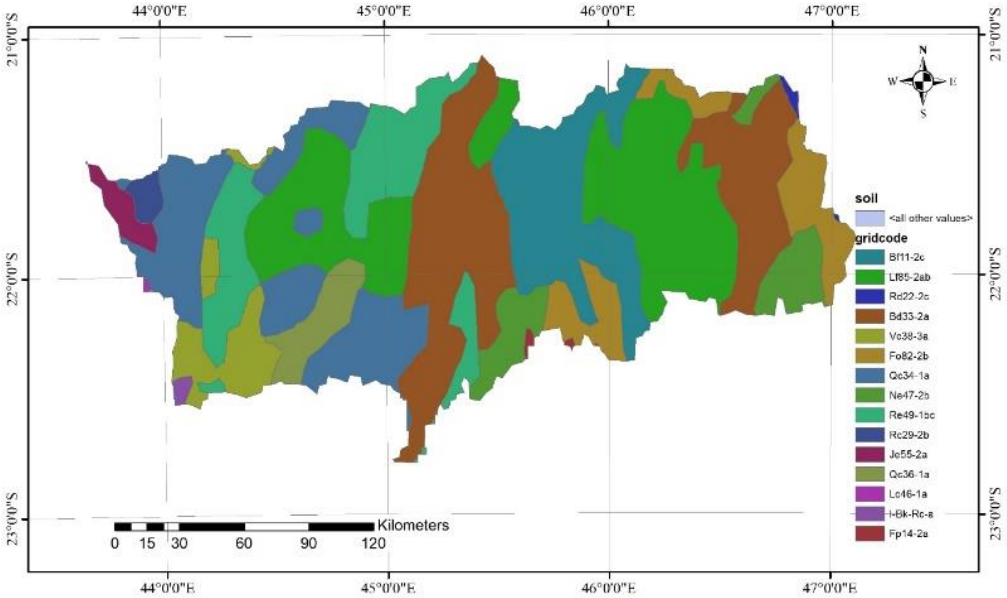

Figure S2. Soil map in Mangoky basin.

Table S2. Soil code and lithology in the Mangoky region.

Soil Code	Associated Soils	Lithology	Hydrologic Soil Group
Bf11-2c	Ferralic cambisol	Granite, Precambrian, amphibolite, pyroxente migmatite, gneiss, Quartenary basalt and acid intrusions	C
Lf85-2ab	Ferric luvisol	Pliocene: Sandstone, sand, clay. Triassic, Jurassic, Cretaceous: sandstne. Permian: schist, migmatite, gneiss	C
Rd22-2c	Dystric regosols	Granite and quartzite. Precambrian: mignatite, gneiss, leptite, pyroxenite, cipolin	C
Bd33-2a	Dystric cambisol	Triassic sandstone: jurassic sandstone; precambrian gneis and migmatite permian schist	C
Vc38-3a	Chromic vertisol	Jurassic marl and limestone. Cretaceous basalt.	D
Fo82-2b	Orthic Ferralsol	Precambrian: migmatite, gneiss, leptite pyroxenite, cipolin; some granitic batholiths	C
Qc34-1a	Cambic arenosols	Pliocene: sand, sandstone, clay. Jurassic and cretaceous: sandstone. Triassic: sandtstone. Often overalain by Quaternary.	
Ne47-2b	Eutric Nitrosols	Precambrian: amphibolitem pyroxenite, cipolin, gneiss, migmatite, Triassic:sandstone	C
Re49-1bc	Eutric regosols	Triassic and Jurassic: sandstone. Precambrian: gneiss and migmatite	C
Rc29-2b	Calcaric regosols	Cretaceous limestone	D
Jc55-2a	Calcaric fluvisols	Quaternary alluvial deposits	C
Qc36-1a	Cambic arenosols	Jurassic sandstone	
Lc46-1a	Chromic luvisols	Eocene limestone	
I-Bk-Re-a	Lithosols	Eocene calcareous sandstone; Jurassic marl	D
Fp14-2a	Plinthic ferralsols	Granite. Precambrian: gneiss, migmatite, leptite, pyroxenite, quartzite	C

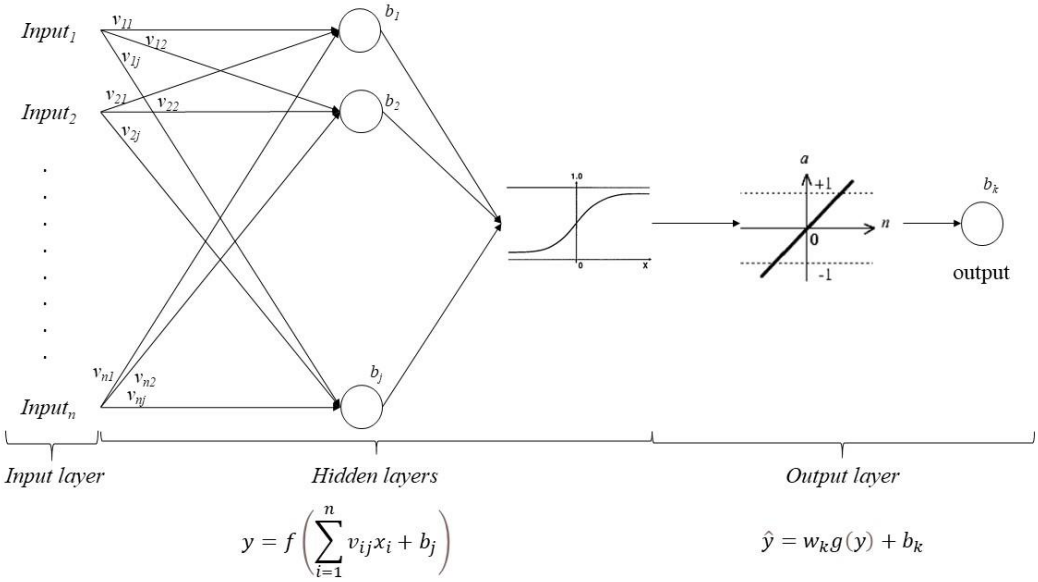

Figure S3. Structure of the ANN developed in this study.

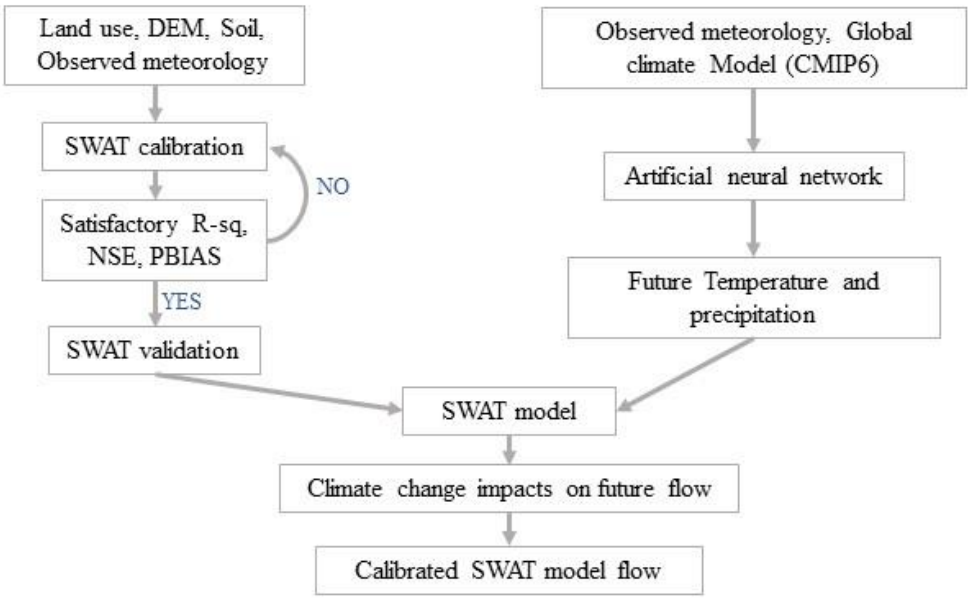

Figure S4. Conceptual model of the present study.

Table S3. Correlation matrix between precipitation, maximum and minimum temperature. Values in bold are different from 0 with a significance level alpha = 0.05.

Variables	prec	Tmax	Tmin
mslp	**−0.3329**	**−0.4316**	**−0.6359**
p_f	**0.1195**	**−0.0578**	**0.1498**
p_u	**0.2644**	**0.4614**	**0.3700**
p_v	**−0.2043**	**−0.3152**	**−0.4003**
p_z	**0.3198**	**0.1268**	**0.3597**
p_th	**−0.2193**	**−0.4480**	**−0.4333**
p_zh	**−0.2236**	**−0.3121**	**−0.3887**
p5_f	**−0.0775**	**−0.4704**	**−0.3863**
p5_u	**−0.0923**	**−0.5199**	**−0.4142**
p5_v	**−0.1639**	**0.1404**	**−0.0430**
p5_z	**−0.1575**	0.0136	**−0.1130**
p5th	**0.0699**	**0.2864**	**0.2254**
p5zh	**−0.1589**	**0.1313**	**−0.0431**
p8_f	**0.2216**	**−0.1163**	**0.1229**
p8_u	**0.2015**	0.0101	**0.0593**
p8_v	**−0.2546**	**−0.1015**	**−0.1650**
p8_z	**−0.1629**	0.0007	**−0.1957**
p8th	**−0.1276**	**−0.0273**	**−0.0391**
p8zh	**−0.2552**	**−0.1317**	**−0.1715**
p500	**−0.0182**	**0.3738**	**0.2339**
p850	**−0.3373**	**−0.2492**	**−0.5038**
r500	**0.4267**	**0.1591**	**0.5282**
r850	**0.2513**	**−0.0377**	**0.2740**
rhum	**0.3306**	**0.2007**	**0.5587**
shum	**0.3505**	**0.5070**	**0.7776**
temp	**0.1103**	**0.6524**	**0.5382**

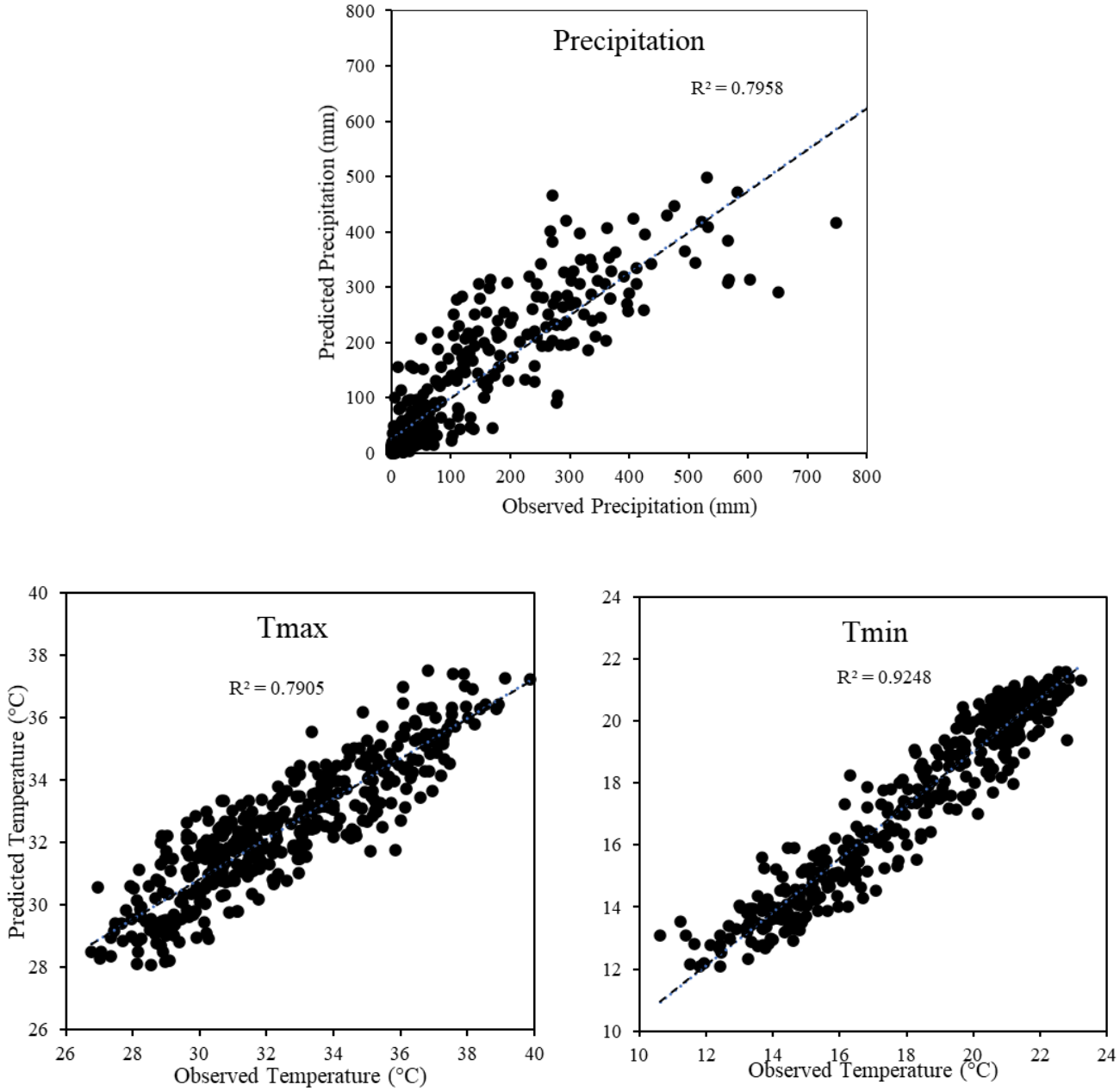

Figure S5. Performance of the ANN (at Station id 214447).

Equation S1. Nash and Sutcliffe efficiency:

$$NSE = \frac{\sum_{i=1}^{N}(Obs_i - Pred_{i)}{}^2}{\sum_{i=1}^{N}(Obs_i - \overline{Obs})^2} \quad (1)$$

Equation S2. PBIAS:

$$PBIAS = \frac{\Sigma_{i=1}^{n}\left(Y_i^{obs} - Y_i^{sim}\right) * 100}{\Sigma_{i=1}^{n} Y_i^{obs}} \quad (2)$$

where Obs_i is the observed data and $Pred_i$ is the predicted data and $\overline{obs}$ is the mean of the observed data. Where Y_i^{obs} is the observed variable, and Y_i^{sim} represents the simulated variable.